

Aiming for Tops of ALPs with a Muon Collider

So Chigusa^{1,2}, Sudhakantha Girmohanta^{3,4},
Yuichiro Nakai^{3,4} and Yufei Zhang^{3,4}

¹*Berkeley Center for Theoretical Physics, Department of Physics,
University of California, Berkeley, CA 94720, USA*

²*Theoretical Physics Group,
Lawrence Berkeley National Laboratory, Berkeley, CA 94720, USA*

³*Tsung-Dao Lee Institute, Shanghai Jiao Tong University,
520 Shengrong Road, Shanghai 201210, China*

⁴*School of Physics and Astronomy, Shanghai Jiao Tong University,
800 Dongchuan Road, Shanghai 200240, China*

Abstract

Future muon colliders with center-of-mass energy of $\mathcal{O}(1-10)$ TeV can provide a clean high-energy environment with advantages in searches for TeV-scale axion-like particles (ALPs), pseudo-Nambu–Goldstone bosons associated with spontaneously broken global symmetries, which are widely predicted in physics beyond the Standard Model (SM). We exploit ALP couplings to SM fermions, and guided by unitarity constraints, build a search strategy focusing on the ALP decay to top quark pairs at muon colliders. It is found that a large parameter space of TeV-scale ALPs with TeV-scale decay constants can be probed by utilizing the ALP-top quark coupling.

1 Introduction

Axion-like particles (ALPs) are pseudo-Nambu–Goldstone bosons (pNGBs) associated with spontaneously broken global symmetries. The exploration of such particles is inspired by the QCD axion [1–3] to solve the strong CP problem [4, 5], but unlike the QCD axion, their masses and decay constants are independent parameters and can vary over a wide range. ALPs are predicted by many extensions of the Standard Model (SM) and naturally arise in string theory [6, 7]. They have various phenomenological, cosmological, and astrophysical implications that have been extensively studied (for reviews, see *e.g.* refs. [8, 9]). Therefore, ALPs are considered to be one of the most important targets in modern particle physics, and their discoveries will make tremendous progress in the understanding of our universe or multiverse.

Among a wide range of ALP models, our focus in the present paper is on ALPs whose masses and decay constants are around the TeV scale. Such TeV-scale ALPs are well-motivated by solutions to the so-called axion quality problem that is a challenge for the Peccei-Quinn (PQ) mechanism to solve the strong CP problem [10–14]. A spontaneously broken global symmetry, resulting in the QCD axion, must be very exact, otherwise, the axion potential would be minimized at an inappropriate value to cancel the strong CP phase. However, any global symmetry is expected to be explicitly broken by quantum gravity effects. Among various possibilities, one approach to the axion quality problem is to increase the axion mass without destroying the PQ solution to the strong CP problem [15–28]. If the axion is heavy enough, quantum gravity effects are no longer problematic, and the axion decay constant can be set to the TeV scale. Another interesting possibility is to consider a warped extra dimension model with three 3-branes where the PQ symmetry is spontaneously broken on the intermediate 3-brane and the electroweak symmetry is broken by Higgs fields localized on the IR brane [29] (for recent developments of multi-brane models, see *e.g.* refs. [30, 31]). This model can address the electroweak naturalness problem and the strong CP problem with a high-quality axion at the same time. A unique prediction of the model is the presence of Kaluza-Klein resonances associated with the invisible QCD axion, which are TeV-scale ALPs with TeV-scale decay constants. Since the parameter space of the ALP mass and decay constant that the Large Hadron Collider (LHC) can explore is limited, new high-energy machines are needed to probe such TeV-scale ALPs.

A future muon collider with center-of-mass (CM) energy of $\mathcal{O}(1-10)$ TeV can furnish a clean high-energy environment with advantages in searches for TeV-scale ALPs. Since the muon is much heavier than the electron and loses much less energy by the synchrotron

radiation, a multi-TeV muon beam with a high luminosity can be realized in a relatively small circular ring. A muon collider is also able to provide clean and precise collisions of point-like particles, unlike hadron colliders that involve composite particles. Due to the short muon lifetime of $2.2\mu\text{s}$ at rest, it is required to produce a large number of muons, cool them down to reduce their emittance, and accelerate them quickly before they decay. Recent technological developments [32–34] make it possible to solve those issues and move forward to the realization of a high-energy muon collider. Therefore, a muon collider has currently received strong support and interest from the particle physics community. For recent studies on the physics reach for a future muon collider, see refs. [35–38] and references therein.

Depending on the structure of ALP couplings to SM particles, ALP production and decay at a high-energy muon collider can vary significantly. The authors of refs. [39, 40] have initiated studies on searches for TeV-scale ALPs coupling to the electroweak gauge bosons, demonstrating that a muon collider can substantially expand the ALP mass coverage. In the present paper, we focus on ALP couplings to SM fermions, which are naturally expected to be present in the axion effective theory. Since the ALP-fermion coupling is proportional to the fermion mass, TeV-scale ALPs predominantly decay into top quark pairs in this scenario. We establish a search strategy for TeV-scale ALPs accordingly; it is demonstrated that the number of jets and reconstructed top candidates can serve as filters to distinguish the signal events we are interested in. We elaborate on the detailed procedure for reducing the principal backgrounds, including beam-induced fake jets. Furthermore, we reconstruct the dijet invariant mass distribution for the outgoing top quark pairs. Searching for a peak structure in the distribution helps to improve the sensitivity, and also provides information about the ALP mass. We employ a likelihood analysis to evaluate the significance of the peak observed in the dijet invariant mass distribution for numerous ALP masses. It is shown that a large parameter space can be probed by utilizing the ALP-top quark coupling.

The rest of the paper is organized as follows. Section 2 introduces the ALP model, presents our setup of ALP couplings to SM particles, and investigates the ALP signal at a muon collider. Then, in section 3, we explain our collider simulations, discuss the event selection strategy, and explain our statistical treatment. The results are presented in section 4. Section 5 is devoted to conclusions and discussions.

2 Setup

This section establishes the effective field theoretic framework for the ALP Lagrangian while elucidating the approximate unitarity constraints associated with its couplings. Subsequently, we consider the production channels within a prospective muon collider, focusing on the direct couplings of ALPs with fermions.

2.1 The effective field theory framework

We define an effective field theory (EFT) by extending the SM with a CP-odd pNGB a , which acts as the ALP and are associated with the breaking of a $U(1)$ global symmetry at a scale f_a . We will work in the SM effective field theory framework, where the electroweak symmetry is realized linearly. The $U(1)$ breaking is assumed to be above the scale of the electroweak symmetry breaking, i.e., $f_a > 250$ GeV so that the effective operators are full $SU(3)_c \otimes SU(2)_L \otimes U(1)_Y$ invariant and ALP couplings to the EW gauge bosons become important for a future muon collider where the vector boson fusion (VBF) processes can be substantial. The Lagrangian can be expanded in powers of a/f_a , to the leading order,

$$\mathcal{L}_{\text{eff}} = \mathcal{L}_{\text{SM}} + \frac{1}{2}(\partial_\mu a)(\partial^\mu a) - \frac{1}{2}m_a^2 a^2 + \delta\mathcal{L}^{(a)}. \quad (2.1)$$

Here, \mathcal{L}_{SM} denotes the ordinary SM Lagrangian, m_a is the ALP mass, and

$$\delta\mathcal{L}^{(a)} = c_{\tilde{W}}\mathcal{A}_{\tilde{W}} + c_{\tilde{B}}\mathcal{A}_{\tilde{B}} + c_{\tilde{G}}\mathcal{A}_{\tilde{G}} + c_{a\Phi}O_{a\Phi}^\psi, \quad (2.2)$$

with

$$O_{a\Phi}^\psi = i\frac{a}{f_a} \sum_{\psi=Q,L} \bar{\psi}_L \mathbf{Y}_\psi \mathbf{\Phi} \sigma_3 \psi_R + \text{h.c.}, \quad (2.3)$$

where $Q_R \equiv (u_R, d_R)$, $L_R \equiv (0, e_R)$, σ_3 acts on the weak isospin, $\mathbf{Y}_Q \equiv \text{diag}(Y_U, Y_D)$, $\mathbf{Y}_L \equiv \text{diag}(0, Y_E)$, and $\mathbf{\Phi} \equiv (\tilde{\Phi}, \Phi)$ with Φ being the SM Higgs doublet and $\tilde{\Phi} = i\sigma_2\Phi^*$. Furthermore, Y_U , Y_D , and Y_E represent the Yukawa coupling matrices in the flavor space for the up-type quarks, down-type quarks, and charged leptons, respectively. In eq. (2.2), $c_{\tilde{W},\tilde{B},\tilde{G},a\Phi}$ are dimensionless coefficients and we have used the notation,

$$\mathcal{A}_{\tilde{X}} = -X_{\mu\nu} \tilde{X}^{\mu\nu} \frac{a}{f_a}, \quad (2.4)$$

for a gauge field $X \in \{B, W, G\}$ with the field strength tensor $X^{\mu\nu}$ and the dual tensor $\tilde{X}^{\mu\nu} = \epsilon^{\mu\nu\rho\sigma} X_{\rho\sigma}$. For the corresponding Feynman rules, see Appendix B of ref. [41].

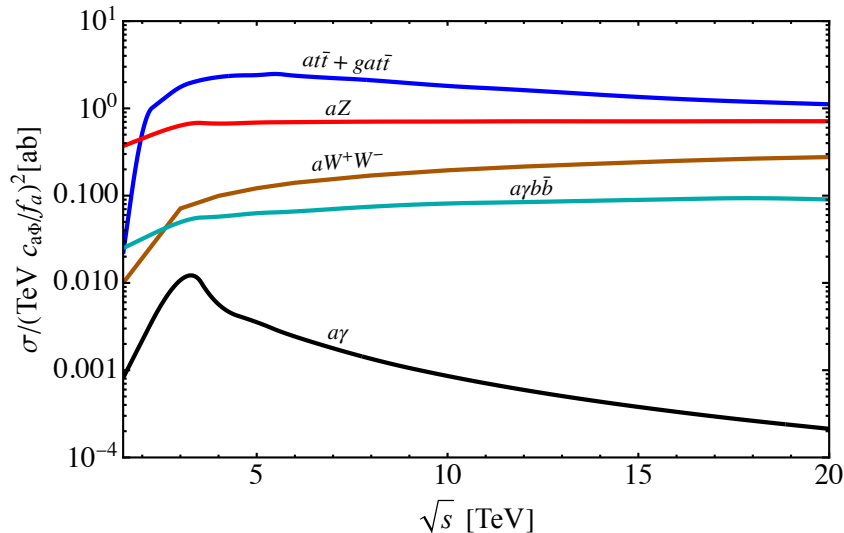


Figure 1: Variation of ALP production cross-sections with CM energy for different channels. We only have non-zero $c_{a\Phi}$, where all the other couplings are set to zero. The plot demonstrates the best channel for the search, namely $\mu^+\mu^- \rightarrow att$.

ALP couplings to the SM vector bosons have played a central role in building ALP search strategies at a future muon collider [39, 40]. On the other hand, the couplings of the ALP to SM fermions were not considered. However, these couplings are natural, and not prohibited by any symmetry principles. Furthermore, the couplings are constrained less stringently by the unitarity bound from partial wave analysis [42]. The helicity amplitude for fermion scattering processes such as $u_k u_{k'} \rightarrow Z a$, where k, k' are flavor indices, places partial-wave unitarity bounds on the direct fermion coupling, the most restrictive of which is [42]

$$|c_{a\Phi}| \lesssim 6 \left(\frac{f_a}{\text{TeV}} \right) \left(\frac{5 \text{ TeV}}{\sqrt{s}} \right). \quad (2.5)$$

The couplings to vector bosons ($c_{\tilde{G}}, c_{\tilde{B}}, c_{\tilde{W}}$) are constrained more stringently from the partial wave unitarity bounds of the scatterings of vector bosons via the ALP (e.g., $ZZ \rightarrow ZZ$).

In the present paper, we initiate the study of ALP search strategies based on the ALP couplings to the SM fermions at a muon collider by focusing on a simplified limit in which the ALP-gauge boson couplings are dialed down to zero, while the effect of the direct couplings to the SM fermions remains. A generic feature of the ALP couplings to the SM fermions, owing to the shift symmetry, is that these couplings are proportional to the corresponding fermion masses. Therefore, an ALP in the TeV mass range dominantly decays to a $t\bar{t}$ pair. This fact drives the search strategy we build in the current study.

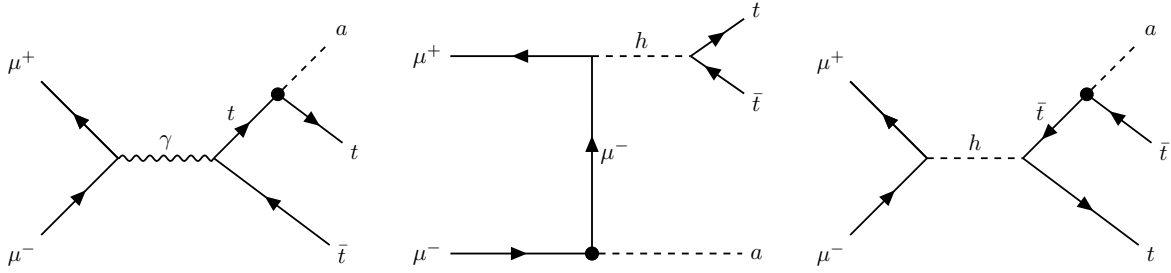


Figure 2: A few representative Feynman diagrams for the signal event $\mu^+\mu^- \rightarrow at\bar{t}$. The final state ALP predominantly decays to a $t\bar{t}$ pair.

2.2 Collider phenomenology

In figure 1, we show the production cross-sections of the ALP for a few representative channels and their variation with CM energy \sqrt{s} of a muon collider. As can be seen in the figure, the top-associated production $\mu^-\mu^+ \rightarrow t\bar{t}a(+g)$, with the matching of jets [43] to avoid double counting, is the dominant production channel for the ALP (see figure 2 for a few representative Feynman diagrams). Note that there are also VBF contributions to the final states including $t\bar{t}a(+g)$, which has a cross-section as large as $\mathcal{O}(10)\%$ of that of $\mu^-\mu^+ \rightarrow t\bar{t}a(+g)$ in spite of the more severe phase space suppression. This can be interpreted as a consequence of the large log factor $\ln(s/\Lambda_W^2)$ with $\Lambda_W = \mathcal{O}(100)$ GeV being the weak scale, which exhibits another role of the muon collider as a vector boson collider. In addition, we have checked that the processes with more than one gluon emission only give $\lesssim 10\%$ correction to the cross-section for $\sqrt{s} = 5$ TeV. Note, however, that these additional QCD processes can be important for larger \sqrt{s} . In the present work, we focus only on the leading production channel $at\bar{t}(+g)$.

Since the ALP couples to the SM fermion with a coupling strength proportional to the Yukawa coupling as shown in eq. (2.3), the ALP most likely decays into a $t\bar{t}$ pair dominantly, when it is kinematically allowed. Moreover, the ALP decays promptly for models with large fermionic couplings of our interest. For example, an illustrative choice for the parameter set, $m_a = 1$ TeV and $|c_{a\Phi}|/f_a = 1/(50 \text{ TeV})$, leads to the branching ratio $\text{Br}(a \rightarrow t\bar{t}) > 99.9\%$ with the partial decay width $\Gamma(a \rightarrow t\bar{t}) \sim 10^{-3} \text{ GeV}$, which corresponds to the typical flight length $c\tau_a \sim 200$ fm with c and τ_a being the speed of light and the ALP lifetime, respectively. Thus, combined with the production process $at\bar{t}$ of our interest, we need to consider a way to look for events with four top quarks.

As explained in detail below, we focus on the hadronic decays of top quarks and

$c_{\tilde{W}}$	$c_{\tilde{B}}$	$c_{\tilde{G}}$	$ c_{a\Phi} /f_a$ [TeV ⁻¹]	m_a [TeV]
0	0	0	6	1

Table 1: A benchmark model parameters we use in our analysis. The coupling value is the maximum of the allowed values for $\sqrt{s} = 5$ TeV from the unitarity bound (2.5).

identify the boosted top-jet candidate by using the reconstructed jet mass. This method effectively selects the top-initiated jets, in which all three hadronic decay products of a single top are within the jet cone. The method works well because of the high collision energy of a muon collider, for example, with $\sqrt{s} = 5$ TeV; in contrast, for four-top events at the LHC with $\sqrt{s} = 14$ TeV, the boosted top-jet reconstruction is not very efficient since the parton-level collision energy is typically $\sqrt{s'} \lesssim$ a few TeV, and the analysis with leptonic decays is more preferable [44–46]. In our analysis, we require at least three top-jet candidates in the event. Therefore, most of the background events come from the $t\bar{t}\bar{t}$ production within the SM, which does not have an axion as an intermediate state. As we will show later in section 3.2, some background events also come from $t\bar{t}$ +jets channels, where a non-top-jet can be misidentified as a top candidate. For reference, table 2 shows the cross-sections of processes relevant to our analysis for the benchmark model of table 1.

3 Analysis

We now describe the event generation process for the signal together with some comments on the reduction of fake jets sourced from the beam-induced backgrounds (BIBs). Then we outline our event selection strategy, considering various potential backgrounds that may arise there. Principal backgrounds are identified and the way to reduce them is explained. Finally, we outline the statistical method to estimate the signal significance.

3.1 Event generation

In the following discussion, we choose $\sqrt{s} = 5$ TeV, $\mathcal{L} = 100$ ab⁻¹, and benchmark parameters shown in table 1 for an illustrative purpose. The events are first generated by MadGraph5 [47], which is further processed by Pythia8 [48] for matching of jets, showering and hadronization. The jet clustering is performed by FastJet [49] with the default clustering parameter $R = 0.5$ and the detector simulation by Delphes [50] using the muon collider detector card [51]. To generate the signal events with an axion in an

	$t\bar{t}a$	$t\bar{t}t\bar{t}$	$t\bar{t}W^+W^-$	$t\bar{t}h$	$t\bar{t}Z$
$\sigma[\text{ab}]$	90	23	465	324	158

Table 2: Cross-sections for the signal and principal backgrounds for the chosen benchmark parameters in table 1.

intermediate state, the model Lagrangian is implemented in FeynRules [52], which then generates a model file compatible with MadGraph5.

As the muon lifetime is $2.2\ \mu\text{s}$ [53] in its rest frame, the decay products of the muon beam and their secondary interactions give rise to the BIBs that pose a major challenge in distinguishing true jets from the beam-induced fake jets. The fake jets have different characteristics from the true jets, which can be exploited to separate them from each other. For example, most of the BIBs have low transverse momenta, asynchronous time of arrival, displaced origin, and high absolute value of pseudo-rapidity. Therefore, the following filtering procedure during the jet reconstruction is shown to efficiently reduce the effect of the BIBs [54]:

- Tracks are filtered by requiring a number of Vertex Detector hits greater than 3 and a number of Inner Tracker hits greater than 2.
- The normalized calorimeter hit time t_N should be within a time window $|t_N| < 250\ \text{ps}$. Here, $t_N \equiv t - t_0 - cD$, with t being the absolute hit time, t_0 the collision time, and D the hit distance from the collision point.
- Each jet should contain at least one track.

Furthermore, the following kinematic cuts are useful to reduce the number of fake jets:

- The pseudo-rapidity cut $|\eta| < 1.5$ to reject most of the fake jets that lie along the beam axis.
- The transverse momentum cut with $p_T > 50\ \text{GeV}$.

According to ref. [54], the filtering procedure has only a mild effect on the real jets with $|\eta| < 1.5$ and $p_T > 50\ \text{GeV}$, leading to the reconstruction efficiency of roughly $\sim 90\%$, while combined with the kinematic cuts it reduces the number of fake jets by orders of magnitude. Thus, in our analysis, we simply assume that the above procedure reduces the effect of the BIBs to a negligible level, and adopt 90% of real jets that pass the kinematic cuts.¹

¹Our approach can be regarded as an approximation that the filtering procedure does not drastically

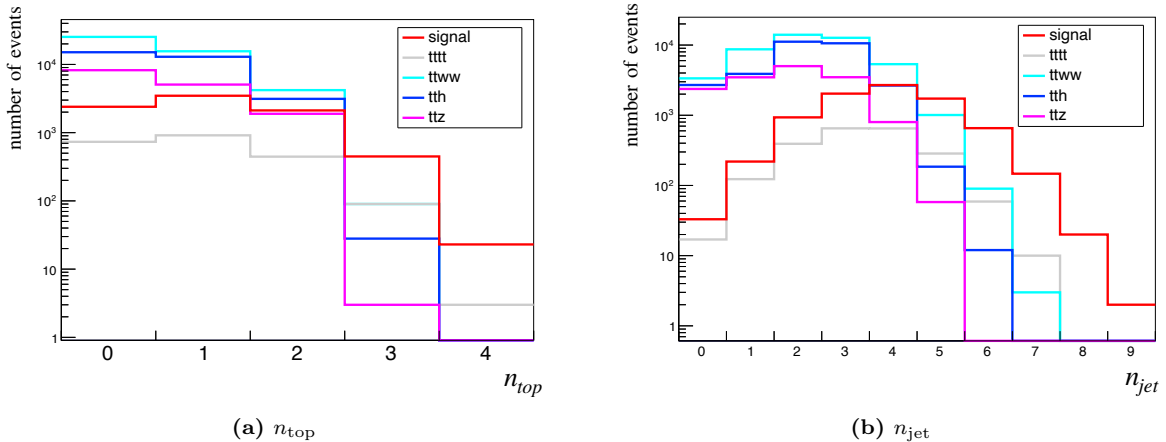


Figure 3: Distribution of signal and background events with respect to the number of top candidates n_{top} (left) and jets n_{jet} (right) defined in the text.

3.2 Event selection

Our general strategy for the event selection is as follows. Firstly, we look for four-top events that contain both contributions from the axion signal and the SM processes. In our analysis, we focus on the hadronic decay of top quarks and identify candidates of boosted top jets using the jet mass information. Then, we utilize the number of top candidates and the number of jets to trim the events with relatively smaller number of top quarks. Finally, we search for a resonance peak structure in the dijet invariant mass distribution of top candidates. Note that the use of boosted top jets under a sufficiently high \sqrt{s} allows us to reconstruct the resonance peak, which is distinct from the search strategy using the leptonic decays in, e.g., ref. [44].

To demonstrate what kind of cuts are useful to reduce the number of background events, we first define the number of top candidates n_{top} and jets n_{jet} for each event. Firstly, n_{jet} corresponds to jets that have passed $|\eta_{\text{jet}}| < 1.5$ and $p_{\text{T,jet}} > 50$ GeV criteria and have been chosen randomly with 90% efficiency as discussed above. Then, among n_{jet} jets in an event, we identify those with mass m_j close to the top mass $m_t \simeq 173$ GeV [53] as top candidates, which counts to be n_{top} . We use the mass window $140 \text{ GeV} < m_j < 220 \text{ GeV}$ for our analysis. In fig. 3, we show the histograms of n_{top} (left) and n_{jet} (right) from the ALP signal as well as some of top-rich SM processes. From the left panel, it is clear that all the SM processes with only two top quarks tend to have $n_{\text{top}} \leq 2$ as expected, so we can significantly reduce the number of background events with the change the kinematic distribution of reconstructed jets. For a more precise treatment, including the effect of the remnant fake jets, we need a full simulation of the BIBs and detector response, which is beyond the scope of the present paper.

cut \ processes	processes				
	$t\bar{t}a$	$t\bar{t}t\bar{t}$	$t\bar{t}W^+W^-$	$t\bar{t}h$	$t\bar{t}Z$
origin	9015	2285	46510	32380	15790
$n_{\text{top}} \geq 3$	495	82	37	26	3
$n_{\text{jet}} \geq 4$	417	65	19	0	0

Table 3: Cutflow for the signal process with benchmark parameters in table 1 and top-rich SM processes for $\sqrt{s} = 5$ TeV.

cut $n_{\text{top}} \geq 3$. Note that even four-top processes tend to have $n_{\text{top}} < 4$ due to the reconstruction efficiency of boosted top jets smaller than 1. From the right panel, it can be seen that the number-of-jet cut, e.g., $n_{\text{jet}} \geq 4$ also helps us to reduce backgrounds while maintaining a large part of the signal events.

Tables 3 and 4 show our cutflow for a simulation of the ALP signal and top-rich SM processes.² Here, we adopt the ALP parameters $m_a = 1$ TeV and $|c_{a\Phi}|/f_a = 6$ TeV⁻¹ as shown in table 1. From tables 3 and 4, we can see that the $n_{\text{top}} \geq 3$ cut significantly reduces the number of events from processes with only two top quarks. The preceding cut $n_{\text{jet}} \geq 4$ further reduces contaminations from $t\bar{t}W^+W^-$ and $t\bar{t}h$ processes, slightly making the signal significance larger. After all cuts are imposed, most of the events are originated from the four-top processes either through the ALP generation or purely SM processes. Note that, from comparison between two tables, it is clear that the top-jet reconstruction efficiency becomes higher when we increase \sqrt{s} from 5 TeV to 10 TeV.

From the cutflow, we can order estimate the reconstruction efficiency of a top quark as a top candidate to be of $\mathcal{O}(10)\%$, while the misidentification rate of the normal jets to be $\mathcal{O}(1)\%$. Using these values, we estimate how many events survive the cut $n_{\text{top}} \geq 3$, focusing on the SM processes with less than two top quarks in the final state, and conclude that contaminations from these processes are negligible for our analysis. Thus, the top-rich processes considered in tables 3 and 4 are the dominant background processes in our analysis. Then, we can see from the tables that the number of ALP signal events can be significantly larger than that of the background events after the cutflow, indicating the efficacy of our approach.

Next, we search for a Gaussian peak in the dijet invariant mass distribution of top

²It turns out that contributions from the VBF processes are negligibly small after our cutflow for both the signal and background events. Thus, we neglect these contributions in the tables and the following analysis.

cut \ processes	$t\bar{t}a$	$t\bar{t}t\bar{t}$	$t\bar{t}W^+W^-$	$t\bar{t}h$	$t\bar{t}Z$
	origin	6625	1509	34970	12300
$n_{\text{top}} \geq 3$	784	146	49	9	61
$n_{\text{jet}} \geq 4$	757	136	24	0	7

Table 4: Same as table 3, but for $\sqrt{s} = 10$ TeV.

jets produced by the ALP decay. Since there are more than two top candidates in the events that passed our cutflow, we need to select two candidates that are most likely sourced from the ALP decay. We have found that the pair of two top quarks closest to each other in the angular space is a good choice. More specifically, we define the variable ΔR , which is the angular separation of the two jets calculated as

$$\Delta R = \sqrt{(\Delta\eta)^2 + (\Delta\phi)^2} , \quad (3.1)$$

where $\Delta\eta$ denotes the pseudo-rapidity difference of the two jets and $\Delta\phi$ is the azimuthal angle between them. We calculate ΔR for every two-jet pair and select the one with the least ΔR . Fig. 4 shows the distribution of the dijet invariant mass m_{jj} of the pair of jets selected as such. We clearly see a peak at $m_{jj} \sim 1$ TeV for the signal events, corresponding to the ALP mass of our choice, while the smooth distribution for $m_{jj} \neq m_a$ is expected to be due to the failure in the choice of two top jets originated from the ALP decay. We find a systematic shift of the peak position slightly lower than m_a , which might come from the missing p_T associated with invisible partons inside jets. However, we comment that the peak position and height could be used to reconstruct the ALP mass m_a and its coupling with a further understanding of the systematic shift by, e.g., a more profound Monte Carlo simulation of the process.

3.3 Statistical treatment

In order to quantify the signal significance taking into account the Gaussian peak structure in the dijet mass distribution shown in fig. 4, we perform fitting of the distribution. Let λ_i be the expected number of events in the i -th bin of the histogram. For the current setup, we decompose λ_i as

$$\lambda_i = b_i + s_i , \quad (3.2)$$

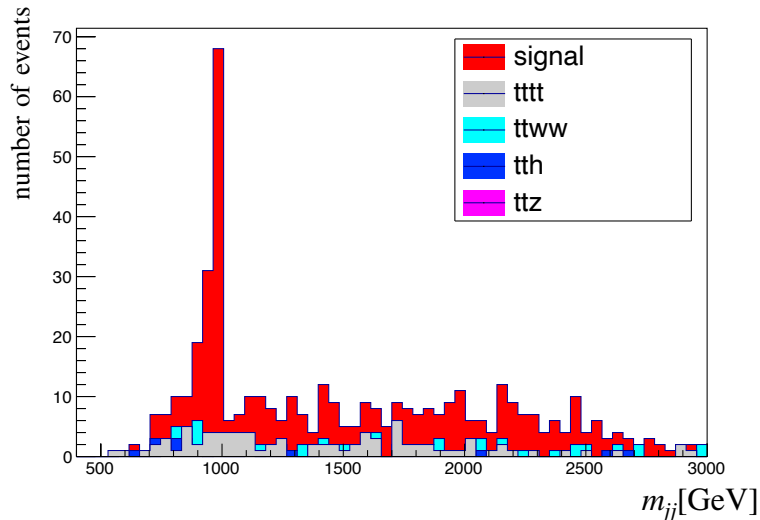


Figure 4: Dijet invariant mass distribution of the two top candidates selected as described in the text.

where b_i denotes the smooth distribution that we model with a cubic function,

$$b_i = \sum_{k=0}^3 \beta_k (m_{jj}^{(i)})^k, \quad (3.3)$$

with $m_{jj}^{(i)}$ being a representative value of m_{jj} for the i -th bin and β_k ($k = 0 \sim 3$) being coefficients, while s_i denotes the peak structure on top of it that we model as

$$s_i = A \exp \left(-\frac{(m_{jj}^{(i)} - m_0)^2}{2\sigma^2} \right). \quad (3.4)$$

Here, A , m_0 , and σ are fitting parameters.

Practically, we first prepare the simulation data for each choice of m_a and the coupling. We fit the data by λ_i with fitting parameters being β_k ($k = 0 \sim 3$), A , m_0 , and σ . Let \tilde{b}_i and \tilde{s}_i be the values of b_i and s_i , respectively, evaluated with the best-fit values of these parameters. Defining their combination,

$$\tilde{\lambda}_i(\mu) = \tilde{b}_i + \mu \tilde{s}_i, \quad (3.5)$$

we treat $\lambda_i(\mu = 1)$ to be the correct expected number of events for the corresponding ALP model to reduce statistical uncertainties of the simulation. Note that \tilde{b}_i not only contains a contribution from the SM processes, but also contains a smooth contribution from the process with an intermediate ALP. This reduces the contribution of the ALP

signal to \tilde{s}_i , but is useful to make the whole procedure robust to any systematic uncertainties that could modify the di-jet mass distribution smoothly. Experimentally, \tilde{b}_i and \tilde{s}_i correspond to the fit result of the sideband region with the smooth distribution (3.3) and that of the whole region with the full expression (3.2).

Let o_i be the histogram data obtained from data. In our analysis, we use $o_i = \tilde{\lambda}_i(\mu = 1)$ as a representative data set. We define the likelihood function as a function of μ as

$$L(\mathbf{o}; \mu) = \prod_{i=1}^{N_B} \frac{e^{-\tilde{\lambda}_i(\mu)} \tilde{\lambda}_i(\mu)^{o_i}}{\Gamma(o_i + 1)}, \quad (3.6)$$

with N_B being the number of bins. We also define a log-likelihood test-statistic,

$$q_0 = -2 \ln \frac{L(\mathbf{o}; \mu = 0)}{L(\mathbf{o}; \mu = 1)}, \quad (3.7)$$

where the choice of $\mu = 1$ maximizes the denominator. According to Wilk's theorem [55], q_0 asymptotically obeys a chi-squared distribution with one degree of freedom. Thus, we identify $\sqrt{q_0} = 5$ as a criteria for the discovery of the ALP model at the 5σ confidence level.

Note that the procedure described so far gives a local significance of the signal for a fixed axion mass m_a used throughout the analysis. For the global p -value, one can define the test-statistic q by making the m_a dependence of the likelihood function explicit and maximizing the denominator of eq. (3.7) by varying μ and m_a at the same time. Since the probability distribution of q is not known a priori, one has to perform a large number of pseudo-experiments to estimate the probability distribution to evaluate the p -value corresponding to the expected value of q . This way to estimate a global p -value is beyond the scope of the current paper and we leave it as a future task.

4 Results

In fig. 5, we show the variation of the test-statistic $\sqrt{q_0}$ as a function of different ALP masses while keeping the coupling fixed to $|c_{a\Phi}|/f_a = 6 \text{ TeV}^{-1}$, which is the maximally allowed value by unitarity for $\sqrt{s} = 5 \text{ TeV}$ as shown in table 1. The assumed collider setup is $\sqrt{s} = 5 \text{ TeV}$ ($\sqrt{s} = 10 \text{ TeV}$) and $\mathcal{L} = 100 \text{ ab}^{-1}$ for the red solid (blue dashed) line. The black dot-dashed line denotes the criteria for the 5σ discovery, which shows that we can probe up to $m_a \sim 1.3 \text{ TeV}$ (2.7 TeV) for $\sqrt{s} = 5 \text{ TeV}$ (10 TeV).

The nature of the curve is understood as follows. Firstly, for m_a barely above the threshold $2m_t$ of having the $a \rightarrow t\bar{t}$ decay channel, top quarks generated from the ALP

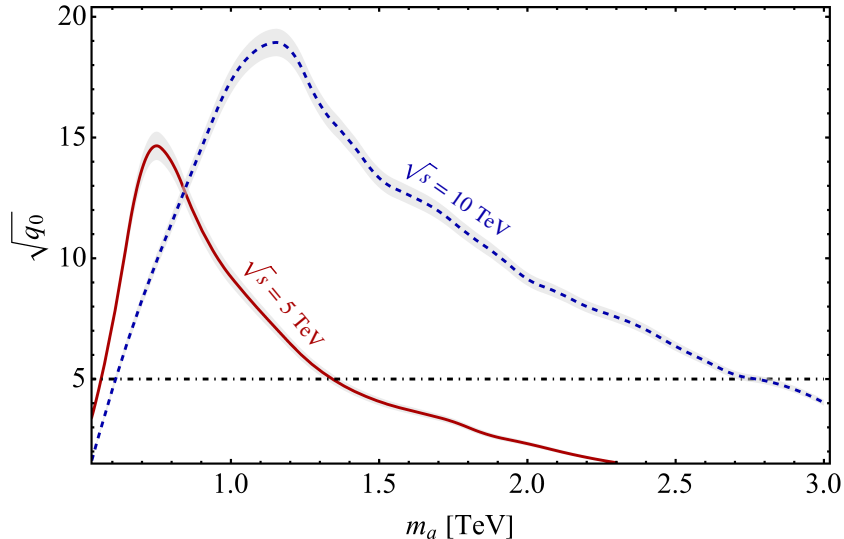


Figure 5: The test-statistic $\sqrt{q_0}$ as a function of the ALP mass m_a for $\sqrt{s} = 5$ TeV (red solid), and $\sqrt{s} = 10$ TeV (blue dashed) and $\mathcal{L} = 100 \text{ ab}^{-1}$ with other model parameters chosen from table 1, while the gray band incorporates the uncertainties in the fitting procedure. The black dot-dashed line denotes $\sqrt{q_0} = 5$ corresponding to the 5σ reach.

decay have small momenta in the ALP-rest frame, and they are highly collimated in the lab frame. Thus, there is a non-negligible probability that hadronic decay products of two top quarks are clustered as a single jet. We confirm this by verifying the existence of a peak at the ALP mass in the jet mass histogram together with a drastic reduction of $n_{\text{top}} = 4$ events in our analysis. This explains the sensitivity decrease for smaller m_a , which is more severe for $\sqrt{s} = 10$ TeV with more collimated top jets and more background events. Note that this sensitivity loss can be well compensated by fitting the jet mass distribution since all the signal events we lose in our analysis should make a more clear peak in the jet mass distribution.

Secondly, for a larger m_a the production cross-section decreases due to the reduction of the available phase space, which basically sets the upper limit on m_a to which our analysis is sensitive. Now, it is useful to understand how this compares with a larger CM energy, as although we do not gain much in the production cross-section as can be inferred from fig. 1, the top-jet reconstruction efficiency increases thanks to higher boost factors. To verify this, and to compare with the case of $\sqrt{s} = 5$ TeV, we set aside the unitarity constraint for the moment, and keep the coupling fixed while increasing CM energy to $\sqrt{s} = 10$ TeV. Clearly, due to increased phase space in the larger ALP mass regime, we can probe to higher values of m_a , and it is also confirmed that one effectively gets more sensitivity, thanks to the enhanced top-jet reconstruction efficiency.

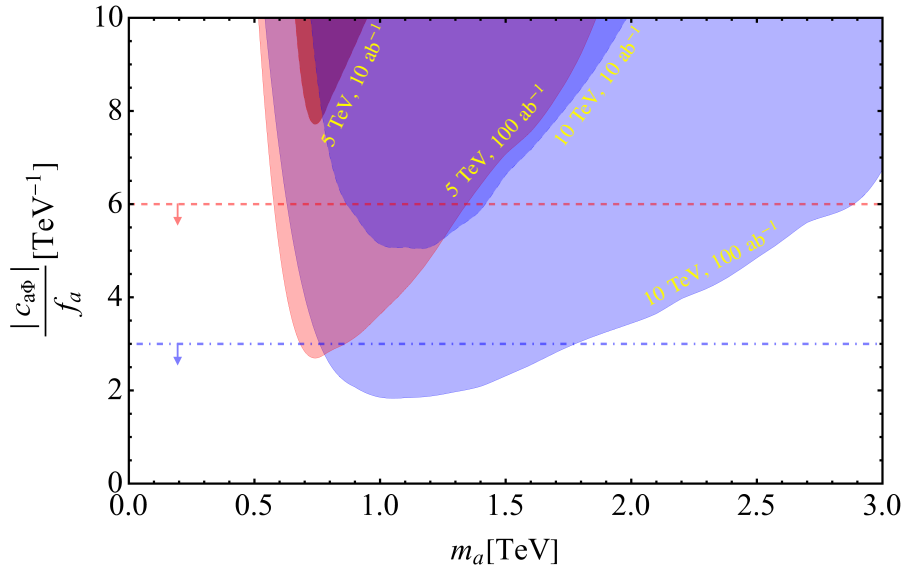


Figure 6: Projected 5σ reach contours in the normalized coupling $|c_{a\Phi}|/f_a$ and m_a plane using the four-top channel search for two different CM energies, namely $\sqrt{s} = 5$ TeV (red) and 10 TeV (blue) for integrated luminosities $\mathcal{L} = 10$ ab^{-1} and 100 ab^{-1} . The approximate unitarity bound [42] is shown as the red dashed (blue dot-dashed) line for $\sqrt{s} = 5$ TeV (10 TeV).

Let us now turn to the following question: what is the 5σ reach for the coupling-mass parameter space, i.e., in the $|c_{a\Phi}|/f_a$ - m_a plane? Note that it is difficult to answer this analytically as the test-statistic does not scale with the coupling, and there are non-trivial effects from the background dependence and top-jet reconstruction efficiencies. Therefore, we utilize the following argument, namely that although the test-statistic does not scale with the coupling, the signal cross-section scales as $(c_{a\Phi}/f_a)^2$. We have verified this numerically within 1% accuracy. This is because once the ALP is produced on-shell, for $m_a > 2m_t$, it immediately decays to two top pairs with $\sim 100\%$ branching fraction. Therefore, we can follow the same technique for evaluating $\sqrt{q_0}$, with the same background as before, while re-scaling the signal events, i.e., a reduction in the coupling will reduce the signal peak, and will result in a reduced $\sqrt{q_0}$. Now we view this procedure as a continuous function of the coupling and extract the value of the coupling at which one gets $\sqrt{q_0} = 5$ for each fixed value of m_a . Hence, this gives the 5σ reach for the normalized coupling for the chosen ALP mass. We repeat this procedure for all the different events generated for distinct m_a , and thereby get the 5σ projected reach in the coupling-mass plane. This is depicted in fig. 6 for two different \sqrt{s} and two different \mathcal{L} . The estimated unitarity bounds are shown for each of the CM energy as dashed lines, and we can see that one is able to probe a large parameter space including the

region where the EFT description is expected to breakdown with possibly the underlying physics signature appearing. For the extra-dimensional KK mode ALP, for example, this could mean that the contribution from the next KK resonance becomes important, while for other UV completion, this could mean the fields that had been integrated out for obtaining the EFT Lagrangian can be excited. We show both the cases for the integrated luminosities 10 ab^{-1} and 100 ab^{-1} that help to elucidate the dependence of the parameter space probe as a function of the luminosity.

5 Discussions

Future muon colliders with CM energy of $\mathcal{O}(1-10)$ TeV are able to provide a clean high-energy environment with advantages in searches for TeV-scale ALPs. We have exploited ALP couplings to the SM fermions, and guided by unitarity constraints, built a search strategy focusing on the ALP decay to SM top quark pairs. We analyzed the extraction of the signal from principal SM backgrounds, and provided a projected sensitivity reach for the parameter space of the ALP.

In our current work, we were agnostic regarding the UV completion, but our search strategy for the four-top channel that we have elucidated here can be applied to specific models to find the reach of future collider machines. Furthermore, the ALP-fermion coupling was considered in isolation to illustrate its effects on the production and decay channel. However, in the future, it will be interesting to consider the gauge boson couplings together with the direct fermion couplings we considered here as this will mimic a more realistic scenario. Regarding the region $2m_b < m_a < 2m_t$, although we do not take up this task in the current work, note that here the $b\bar{b}$ decay channel for the ALP decay will dominate, and a similar search strategy could be followed to project a constraint in this regime. We also note that High-Luminosity (HL)-LHC will have a comparable or better handle at this mass range, and one can do a comparative analysis of the efficacy of HL-LHC and a future lepton collider for this regime, and we relegate it to a future work.³ To conclude, our results show that the ALP-top coupling can be crucial to probe the ALP in four-top channels, as this coupling is natural from a UV theory perspective and can provide a complementary or even better chance at probing it in a future muon collider machine to the more investigated channels involving gauge boson couplings primarily [39, 40].

³Four-top events have been detected recently at both ATLAS and CMS [44–46].

Acknowledgements

SC is supported by the Director, Office of Science, Office of High Energy Physics of the U.S. Department of Energy under the Contract No. DE-AC02-05CH1123. YN is supported by Natural Science Foundation of China under grant No. 12150610465.

References

- [1] R. D. Peccei and H. R. Quinn, *CP Conservation in the Presence of Instantons*, *Phys. Rev. Lett.* **38** (1977) 1440.
- [2] S. Weinberg, *A New Light Boson?*, *Phys. Rev. Lett.* **40** (1978) 223.
- [3] F. Wilczek, *Problem of Strong P and T Invariance in the Presence of Instantons*, *Phys. Rev. Lett.* **40** (1978) 279.
- [4] C. A. Baker et al., *An Improved experimental limit on the electric dipole moment of the neutron*, *Phys. Rev. Lett.* **97** (2006) 131801 [[hep-ex/0602020](#)].
- [5] J. M. Pendlebury et al., *Revised experimental upper limit on the electric dipole moment of the neutron*, *Phys. Rev. D* **92** (2015) 092003 [[1509.04411](#)].
- [6] P. Svrcek and E. Witten, *Axions In String Theory*, *JHEP* **06** (2006) 051 [[hep-th/0605206](#)].
- [7] A. Arvanitaki, S. Dimopoulos, S. Dubovsky, N. Kaloper and J. March-Russell, *String Axiverse*, *Phys. Rev. D* **81** (2010) 123530 [[0905.4720](#)].
- [8] J. Beacham et al., *Physics Beyond Colliders at CERN: Beyond the Standard Model Working Group Report*, *J. Phys. G* **47** (2020) 010501 [[1901.09966](#)].
- [9] K. Choi, S. H. Im and C. Sub Shin, *Recent Progress in the Physics of Axions and Axion-Like Particles*, *Ann. Rev. Nucl. Part. Sci.* **71** (2021) 225 [[2012.05029](#)].
- [10] R. Holman, S. D. H. Hsu, T. W. Kephart, E. W. Kolb, R. Watkins and L. M. Widrow, *Solutions to the strong CP problem in a world with gravity*, *Phys. Lett. B* **282** (1992) 132 [[hep-ph/9203206](#)].
- [11] M. Kamionkowski and J. March-Russell, *Planck scale physics and the Peccei-Quinn mechanism*, *Phys. Lett. B* **282** (1992) 137 [[hep-th/9202003](#)].

- [12] S. M. Barr and D. Seckel, *Planck scale corrections to axion models*, *Phys. Rev. D* **46** (1992) 539.
- [13] S. Ghigna, M. Lusignoli and M. Roncadelli, *Instability of the invisible axion*, *Phys. Lett. B* **283** (1992) 278.
- [14] L. M. Carpenter, M. Dine and G. Festuccia, *Dynamics of the Peccei Quinn Scale*, *Phys. Rev. D* **80** (2009) 125017 [[0906.1273](#)].
- [15] S. Dimopoulos, *A Solution of the Strong CP Problem in Models With Scalars*, *Phys. Lett. B* **84** (1979) 435.
- [16] B. Holdom and M. E. Peskin, *Raising the Axion Mass*, *Nucl. Phys. B* **208** (1982) 397.
- [17] M. Dine and N. Seiberg, *String Theory and the Strong CP Problem*, *Nucl. Phys. B* **273** (1986) 109.
- [18] J. M. Flynn and L. Randall, *A Computation of the Small Instanton Contribution to the Axion Potential*, *Nucl. Phys. B* **293** (1987) 731.
- [19] V. A. Rubakov, *Grand unification and heavy axion*, *JETP Lett.* **65** (1997) 621 [[hep-ph/9703409](#)].
- [20] Z. Berezhiani, L. Gianfagna and M. Giannotti, *Strong CP problem and mirror world: The Weinberg-Wilczek axion revisited*, *Phys. Lett. B* **500** (2001) 286 [[hep-ph/0009290](#)].
- [21] H. Fukuda, K. Harigaya, M. Ibe and T. T. Yanagida, *Model of visible QCD axion*, *Phys. Rev. D* **92** (2015) 015021 [[1504.06084](#)].
- [22] T. Gherghetta, N. Nagata and M. Shifman, *A Visible QCD Axion from an Enlarged Color Group*, *Phys. Rev. D* **93** (2016) 115010 [[1604.01127](#)].
- [23] S. Dimopoulos, A. Hook, J. Huang and G. Marques-Tavares, *A collider observable QCD axion*, *JHEP* **11** (2016) 052 [[1606.03097](#)].
- [24] P. Agrawal and K. Howe, *Factoring the Strong CP Problem*, *JHEP* **12** (2018) 029 [[1710.04213](#)].
- [25] M. K. Gaillard, M. B. Gavela, R. Houtz, P. Quilez and R. Del Rey, *Color unified dynamical axion*, *Eur. Phys. J. C* **78** (2018) 972 [[1805.06465](#)].

- [26] A. Hook, S. Kumar, Z. Liu and R. Sundrum, *High Quality QCD Axion and the LHC*, *Phys. Rev. Lett.* **124** (2020) 221801 [[1911.12364](#)].
- [27] T. Gherghetta, V. V. Khoze, A. Pomarol and Y. Shirman, *The Axion Mass from 5D Small Instantons*, *JHEP* **03** (2020) 063 [[2001.05610](#)].
- [28] T. Gherghetta and M. D. Nguyen, *A Composite Higgs with a Heavy Composite Axion*, *JHEP* **12** (2020) 094 [[2007.10875](#)].
- [29] S. J. Lee, Y. Nakai and M. Suzuki, *High quality axion via a doubly composite dynamics*, *JHEP* **03** (2022) 038 [[2112.08083](#)].
- [30] S. J. Lee, Y. Nakai and M. Suzuki, *Multiple hierarchies from a warped extra dimension*, *JHEP* **02** (2022) 050 [[2109.10938](#)].
- [31] S. Girmohanta, S. J. Lee, Y. Nakai and M. Suzuki, *Multi-brane cosmology*, [2304.05586](#).
- [32] MICE collaboration, *Demonstration of cooling by the Muon Ionization Cooling Experiment*, *Nature* **578** (2020) 53 [[1907.08562](#)].
- [33] J. P. Delahaye, M. Diemoz, K. Long, B. Mansoulié, N. Pastrone, L. Rivkin et al., *Muon Colliders*, [1901.06150](#).
- [34] N. Bartosik et al., *Detector and Physics Performance at a Muon Collider*, *JINST* **15** (2020) P05001 [[2001.04431](#)].
- [35] H. Al Ali et al., *The muon Smasher's guide*, *Rept. Prog. Phys.* **85** (2022) 084201 [[2103.14043](#)].
- [36] K. M. Black et al., *Muon Collider Forum Report*, [2209.01318](#).
- [37] C. Aime et al., *Muon Collider Physics Summary*, [2203.07256](#).
- [38] Y. Hamada, R. Kitano, R. Matsudo, H. Takaura and M. Yoshida, μ TRISTAN, *PTEP* **2022** (2022) 053B02 [[2201.06664](#)].
- [39] T. Han, T. Li and X. Wang, *Axion-Like Particles at High Energy Muon Colliders – A White paper for Snowmass 2021*, in *2022 Snowmass Summer Study*, 3, 2022, [2203.05484](#).
- [40] Y. Bao, J. Fan and L. Li, *Electroweak ALP Searches at a Muon Collider*, [2203.04328](#).

- [41] I. Brivio, M. B. Gavela, L. Merlo, K. Mimasu, J. M. No, R. del Rey et al., *ALPs Effective Field Theory and Collider Signatures*, *Eur. Phys. J. C* **77** (2017) 572 [[1701.05379](#)].
- [42] I. Brivio, O. J. P. Éboli and M. C. Gonzalez-Garcia, *Unitarity constraints on ALP interactions*, *Phys. Rev. D* **104** (2021) 035027 [[2106.05977](#)].
- [43] S. Frixione and B. R. Webber, *Matching NLO QCD computations and parton shower simulations*, *JHEP* **06** (2002) 029 [[hep-ph/0204244](#)].
- [44] ATLAS collaboration, *Measurement of the $t\bar{t}$ production cross section in pp collisions at $\sqrt{s} = 13$ TeV with the ATLAS detector*, *JHEP* **11** (2021) 118 [[2106.11683](#)].
- [45] ATLAS collaboration, *Observation of four-top-quark production in the multilepton final state with the ATLAS detector*, *Eur. Phys. J. C* **83** (2023) 496 [[2303.15061](#)].
- [46] CMS collaboration, *Observation of four top quark production in proton-proton collisions at $\sqrt{s} = 13$ TeV*, [2305.13439](#).
- [47] J. Alwall, R. Frederix, S. Frixione, V. Hirschi, F. Maltoni, O. Mattelaer et al., *The automated computation of tree-level and next-to-leading order differential cross sections, and their matching to parton shower simulations*, *JHEP* **07** (2014) 079 [[1405.0301](#)].
- [48] C. Bierlich et al., *A comprehensive guide to the physics and usage of PYTHIA 8.3*, [2203.11601](#).
- [49] M. Cacciari, G. P. Salam and G. Soyez, *FastJet User Manual*, *Eur. Phys. J. C* **72** (2012) 1896 [[1111.6097](#)].
- [50] DELPHES 3 collaboration, *DELPHES 3, A modular framework for fast simulation of a generic collider experiment*, *JHEP* **02** (2014) 057 [[1307.6346](#)].
- [51] M. Selvaggi, “Talk at mdi studies meeting of the muon collider collaboration.” https://indico.cern.ch/event/957299/contributions/4023467/attachments/2106044/3541874/delphes_card_mucol_mdi%20.pdf.
- [52] A. Alloul, N. D. Christensen, C. Degrande, C. Duhr and B. Fuks, *FeynRules 2.0 - A complete toolbox for tree-level phenomenology*, *Comput. Phys. Commun.* **185** (2014) 2250 [[1310.1921](#)].

- [53] PARTICLE DATA GROUP collaboration, *Review of Particle Physics*, [PTEP **2022** \(2022\) 083C01](#).
- [54] MUON COLLIDER collaboration, *Simulated Detector Performance at the Muon Collider*, [2203.07964](#).
- [55] S. S. Wilks, *The Large-Sample Distribution of the Likelihood Ratio for Testing Composite Hypotheses*, [The Annals of Mathematical Statistics **9** \(1938\) 60](#) .